Structural and Dielectric Properties of $Li_{0.5}Bi_{0.5}Ti_{0.8}Zr_{0.2}O_3$ Ceramics

D. Panda[1], B. B. Mohanty[2*], P. S. Sahoo[3], R. N. P. Choudhary[4]

[1]PXE, DRDO, Chandipur, Balasore, Orissa, India
[2]Department of Physics, Betnoti College Betnoti, Mayurbhanj, Orissa, India
[3]Department of Physics, North Orissa University, Baripada, Odisha, India
[4]Department of Physics ITER, Bhubaneswar, Odisha, India
Email: *banabihari4u@gmail.com

Abstract

A polycrystalline orthorhombic compound of $Li_{0.5}Bi_{0.5}Ti_{0.8}Zr_{0.2}O_3$ is synthesized by using a high temperature solid-state reaction technique at high temperature (*i.e.*, at 900˚C). The room temperature X-ray diffraction study assured the evolution of single-phase compound with orthorhombic structure. The dielectric analysis of $Li_{0.5}Bi_{0.5}Ti_{0.95}Zr_{0.05}O_3$ explored over a broad frequency range (10^3 - 10^6 Hz) at various temperatures (33˚C - 500˚C) displayed that the dielectric properties of the material are dependent on both frequency and temperature. Dielectric study reveals that the ferro to paraelectric phase transition of the studied compound is a temperature of 112˚C. The nature of the variation of conductivity and value of activation energy in different regions, calculated from the temperature dependence of ac conductivity suggest that the conduction process is of mixed type (*i.e.*, ionic–polaronic and space charge generated from the oxygen ion vacancies).

Subject Areas

Condensed State Physics

Keywords

Ceramics, Perovskite Structure, Solid-State Reaction, X-Ray Diffraction

1. Introduction

The discovery of ferroelectricity in $BaTiO_3$ is very crucial for the material researchers. Oxides of disparate structures like tungsten bronze, perovskite, layer structure etc., were analysed for application in numerous devices such as transducers, actuators, multi-layer capacitors, ferroelectric random-access memory

and display, microwave dielectric resonators, etc. This galvanized the scientists to flourish thermally well-built modern electronic materials possessing high dielectric constant and low dielectric loss. Reckoning the above, the ferroelectric oxides of perovskite structural family have chiefly been probed for their convenient dielectric [1], electro-optic [2], nonlinear optic [3] pyroelectric [4], piezoelectric [5] properties. A perfect perovskite structure can be represented by a general formula as ABO_3 where A is a large cation (mono to trivalent) and B is a small cation (a transition metal ion). The A ions occupy the corners of the cube, which is 12 coordinated, while the B ions sit on the body center positions inside an oxygen octahedron, which are at the face center positions. Literature survey disclosed that an ample of research has been accomplished on perovskite type ferroelectric oxides niobates and tantalates [6] [7] [8]. We could not find any, but no work is executed on the structural, dielectric and electrical properties of current compound. Looking to the importance of the material, we have synthesised and analysed the structural and dielectric properties of a new compound having the chemical formula $Li_{0.5}Bi_{0.5}Ti_{0.8}Zr_{0.2}O_3$ (LBTZ).

2. Experimental

2.1. Material Preparation

The polycrystalline sample $Li_{0.5}Bi_{0.5}Ti_{0.8}Zr_{0.2}O_3$ (LBTZ) was prepared with apposite stoichiometric ratio of precursors; $LiCO_3$, Bi_2O_3, TiO_2, ZrO_2 of high purity (>99.9%) were weighed and blended mechanically by an agate mortar for about 3 h. The powders were then calcined at optimized temperature and time (900°C for 12 h) in air condition. The calcined powder thus procured was blended with PVA (poly vinyl alcohol) binder, grinded and were palletized ensuingly (about 10 mm in diameter and 1 - 2 mm thickness) under uniaxial pressure of 4 × 106 N/m². Thereafter the pellets were sintered in air atmosphere at 950°C for 12 h. Ultimately the pellets were laminated with high purity silver paint, and then heated at 150°C for 2 h before executing the electrical measurements.

2.2. Material Charecterisation

X-ray diffraction (XRD) pattern of the material procured in a vast range of Bragg angle 2θ ($200 \le 2\theta \le 800$) at a scanning speed of 30 min⁻¹ by an X-ray diffractometer (Rigaku, Miniflex) with CuKα radiation (λ = 1.5405 Å) at room temperature. The surface morphology of the pellet sample of the material was recorded with a high-resolution scanning electron microscope (SEM: JOEL-JSM model: 5800F). The dielectric characterisation of the sample was prosecuted in the temperature range of 32°C - 5000°C and frequency range of 1 kHz to 1 MHz, using a computer-controlled Hioki HiTester LCR meter.

3. Results and Discussion

3.1. Structural and Microstructural Analysis

Figure 1 shows the XRD pattern of the sample. Indexing of all the peaks of the
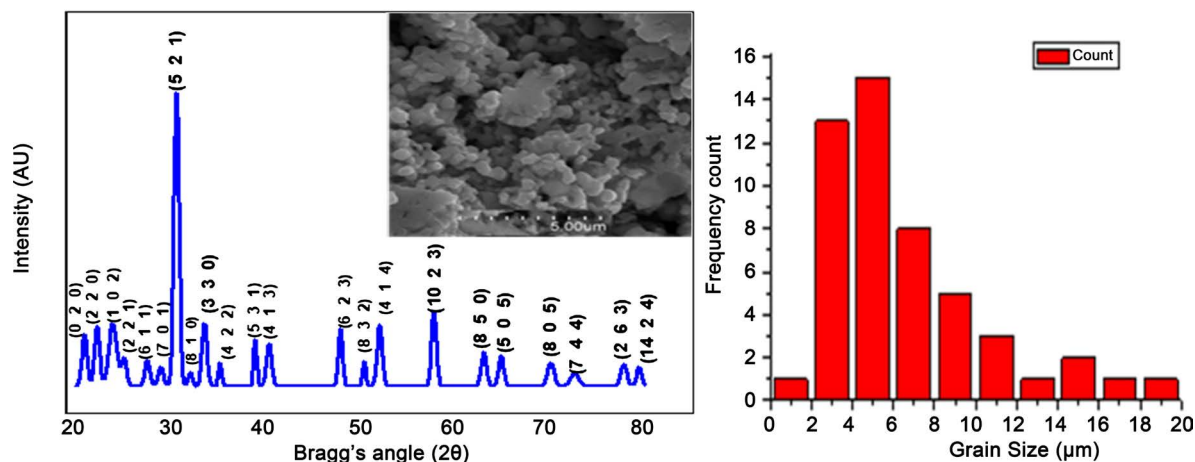
Figure 1. Room temperature XRD pattern (left), SEM (inset) and histogram (right) of $Li_{0.5}Bi_{0.5}Ti_{0.8}Zr_{0.2}O_3$ ceramics.

pattern were done taking their 2θ values bya computer program package, "POWDMULT" [9] in distinct crystal system and cell configuration and are traced to be sharp and solo, which The peaks are discrete from those of ingredients ensuring the evolution of new single-phase compound. On the basis of the best agreement (based on least-squares refinement) between scrutinised (obs) and reckoned (cal) interplaner distance d (*i.e.*, $\Sigma(d_{obs} - d_{cal})$ = minimum), an orthorhombic unit cell was selected with lattice parameters: a = 18.8065 (29) Å, b = 8.3211 (29), c = 8.2920 (29) Å (estimated standard deviation in parentheses) which are consistence with the reported ones [10]. The coherently average dispersed crystallite size (D) of the compound was computed to be ~ 15 nm using Scherrer's equation; D = $0.89\lambda/(\beta_{1/2}\cos\theta_{hkl})$, where λ = 1.5405 Å and $\beta_{1/2}$ = peak width of the reflection at half maxima [11]. The contributions of strain, instrumental error and other unknown effects in the peak broadening has not been taken into board during the crystallite size enumeration.

The room temperature SEM micrograph (**Figure 1** (inset)) of the LBTZ compound, confirmed homogenously and non-uniform distribution of the grains over the entire surface of the sample. The grain size evaluated from the histogram **Figure 1** (right) is traced to be of 4.9 μm. As expected, the grain size of the sample obtained here is gigantic in comparison to the crystallite size enumerated from Scherrer's equation. Thus, a solo grain has large number of crystallites [12].

3.2. Dielectric Analysis

The temperature variation of relative dielectric constant (ε_r) at some selected frequencies of compound is shown **Figure 2**. The plot firmly established the ferro to paraelectric phase transition at 112˚C. The value of ε_r is small at low temperatures which increases with rise in temperature. The dielectric constant (ε_r) at frequencies 10, 50, 100, 500 and 1000 kHz are found to be 225, 203, 159, 145 and 125 respectively at the transition temperature. The variation of $\tan\delta$ follows the same pattern as that of ε_r. The increase in the value of $\tan\delta$ may be due to (i) enhancement in the conductivity and (ii) reduction in the contribution of

ferroelectric domain wall [13].

3.3. Ac Conductivity Analysis

The ac electrical conductivity (σ_{ac}) is calculated using the dielectric data and an empirical relation. $\sigma_{ac} = \omega \varepsilon_r \varepsilon_0 \tan\delta$, where ε_0 = permittivity of free space and ω = angular frequency. Figure 3 shows the variation of σ_{ac} as a function of temperature at frequencies 10 and 100 kHz.

The nature of the variation (Figure 3) is almost linear over a wide temperature region obeying the Arrhenius relation: $\sigma_{ac} = \sigma_0 \exp(-E_a/k_B T)$ [14], Each of graph is divided into two different regions independently of frequency. Every divided region is characterized by different slopes showing different activation energy. The solid line of figure shows the linear fit. The activation energy calculated from the slope of the curve at different temperatures has been compared in Table 1. Due to the dielectric phase transitions, abnormality in conductivity was
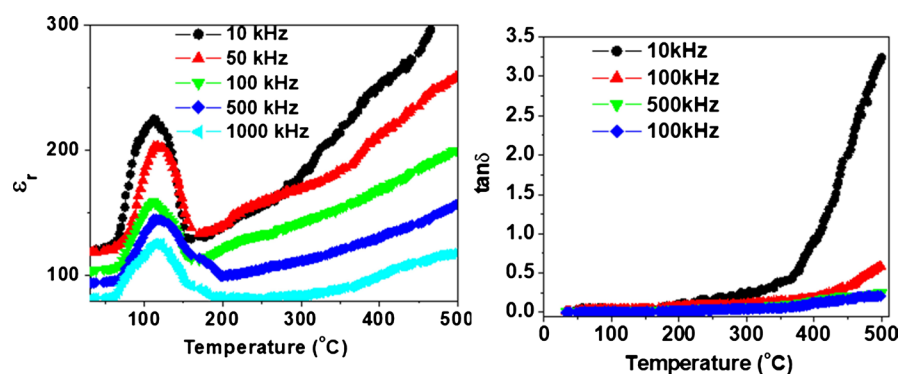
Figure 2. Variation of ε_r and $\tan\delta$ (right) with temperature of $Li_{0.5}Bi_{0.5}Ti_{0.8}Zr_{0.2}O_3$ at some selected frequencies.
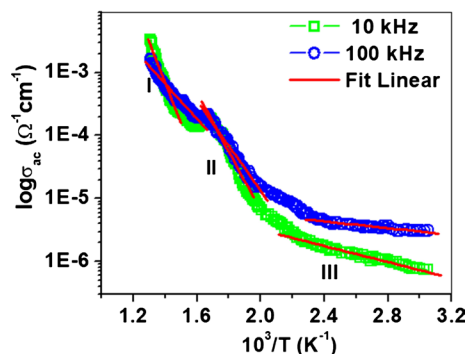
Figure 3. Variation of σ_{ac} with 1000/T of $Li_{0.5}Bi_{0.5}Ti_{0.8}Zr_{0.2}O_3$ at two selected frequencies.

Table 1. Comparison of activation energy Ea (eV) of $Li_{0.5}Bi_{0.5}Ti_{0.8}Zr_{0.2}O_3$ at two different frequencies in region I, II and III, calculated from σ_{ac} vs. 1/T graphs.

Frequency (kHz)	Activation energy E_a (eV)		
	Region I	Region II	Region III
10	1.29	0.93	0.13
1000	0.56	0.71	0.52

observed for all the compound at temperatures nearly equal to its Curie temperature, which might be due to the dielectric phase transition. The value of σ_{ac} increases with increase in temperature indicating negative temperature coefficient of resistance (NTCR) behavior. The increase in conductivity is due to the hopping action of the ions because of thermally activated electrons. At high temperature higher value of activation energy indicates that conductivity is for the movement of oxygen vacancies. Activation energy is low at high frequency as compared to that at the low frequency (Table 1). This is because at low frequencies the overall conductivity is the result of hopping of charge carriers over a large distance and at higher frequencies is restricted to only nearest neighboring defects sites [15].

4. Conclusion

The polycrystalline sample of LBTZ was prepared by a solid-state-reaction route. Preliminary X-ray analysis confirms the single phase orthorhombic crystal structure at room temperature. The plot firmly established the ferro to paraelectric phase transition at 112°C. The dielectric constant of the ceramics decreases with increasing frequency. The activation energy of the compound was found to be different in different regions indicating presence of different conduction mechanisms.

Acknowledgements

Conflicts of Interest

The authors declare no conflicts of interest regarding the publication of this paper.

References

[1] Zhu, X.L., Chen, X.M., Liu, X.Q. and Yuan, Y. (2006) Dielectric Characteristics and Diffuse Ferroelectric Phase Transition in $Sr_4La_2Ti_4Nb_6O_{30}$ Tungsten Bronze Ceramics. *Journal of Materials Research*, **21**, 1787-1792.
https://doi.org/10.1557/jmr.2006.0201

[2] Huang, C., Bhalla, A.S. and Guo, R. (2005) Measurement of Microwave Electro-Optic Coefficient in Sr0.61Ba0.39Nb2O6 Crystal Fiber. *Applied Physics Letters*, **86**, Article ID: 211907. https://doi.org/10.1063/1.1937997

[3] Ramirez, M.O., Jaque, D., Bausa, L.E., Sole Garci, J. and Kaminskii, A.A. (2005) Near Infraredand Visible Tunability from a Diode Pumped Nd Activated Strontium

Barium Niobate Laser Crystal. *Physical Review Letters*, **95**, Article ID: 267401.

[4] Rao, K.S. and Nath, N.V. (2005) Influence of Rare-Earth Ion on Piezoelectric and Pyroelectric Properties of PBN System. *Ferroelectrics*, **325**, 15-24.
https://doi.org/10.1080/00150190500326605

[5] Jiang, W., Cao, W., Yi, X. and Chen, H. (2005) The Elastic and Piezoelectric Properties of Tungsten Bronze Ferroelectric Crystals $(Sr_{0.7}Ba_{0.3})2NaNb_5O_{15}$ and $(Sr_{0.3}Ba_{0.7})2NaNb_5O_{15}$. *Journal of Applied Physics*, **97**, Article ID: 094106.
https://doi.org/10.1063/1.1881777

[6] Raju, M.R. and Choudhary, R.N.P. (2006) Effect of Zr Substitution on Structural, Dielectric and Electrical Properties of $Sr_5SmTi_3Nb_7O_{30}$ Ceramics. *Materials Chemistry and Physics*, **99**, 135-143. https://doi.org/10.1016/j.matchemphys.2005.09.084

[7] Chen, W., Kinemuchi, Y., Watari, K., Tamura, T. and Miwa, K. (2006) Preparation of Grain‐Oriented $Sr_{0.5}Ba_{0.5}Nb_2O_6$ Ferroelectric Ceramics by Magnetic Alignment. *Journal of the American Ceramic Society*, **89**, 381-384.
https://doi.org/10.1111/j.1551-2916.2005.00694.x

[8] Ko, H., Kojima, S., Lushnikov, S.G., Katiyar, R.S., Kim, T.-H. and Ro, J.-H. (2002) Low-Temperature Transverse Dielectric and Pyroelectric Anomalies of Uniaxial Tungsten Bronze Crystals. *Journal of Applied Physics*, **92**, 1536.
https://doi.org/10.1063/1.1491995

[9] Wu, E. (1989) POWD, an Interactive Powder Diffraction Data Interpretation and Index Program. Ver.2.1. School of Physical Science, Flinders University South Bedford Park, Australia.

[10] Geiss, E.A., Scott, B.A., Burns, G., O'Kane, D.F. and Segmuller, A. (1969) Alkali Strontium-Barium-Lead Niobate Systems with a Tungsten Bronze Structure: Crystallographic Properties and Curie Points. *Journal of the American Ceramic Society*, **52**, 276-281. https://doi.org/10.1111/j.1151-2916.1969.tb09183.x

[11] Klug, H.P. and Alexander, L.E. (1974) X-Ray Diffraction Procedures for Polycrystalline and Amorphous Materials. Willey-Interscience, New York.

[12] Sahho, P.S., Panigrahi, A., Patri, S.K. and Choudhary, R.N.P. (2010) Impedance Spectroscopy of $Ba_3Sr_2DyTi_3V_7O_{30}$ Ceramic. *Bulletin of Materials Science*, **33**, 129-134. https://doi.org/10.1007/s12034-010-0018-8

[13] Dash, S., Choudhary, R.N.P. and Kumar, A. (2014) Impedance Spectroscopy and Conduction Mechanism of Multiferroic $(Bi_{0.6}K_{0.4})(Fe_{0.6}Nb_{0.4})O_3$. *Journal of Physics and Chemistry of Solids*, **75**, 1376-1382. https://doi.org/10.1016/j.jpcs.2014.07.018

[14] Singh, A.K., Barik, S.K., Choudhary, R.N.P. and Mahapatra, P.K. (2009) Ac Conductivity and Relaxation Mechanism in $Ba_{0.9}Sr_{0.1}TiO_3$. *Journal of Alloys and Compounds*, **479**, 39-42. https://doi.org/10.1016/j.jallcom.2008.12.130

[15] Bhattacharya, S., Bharadwaj, S.S.N. and Krupanidhi, S.B. (2000) Alternating Current Conduction Behavior of Excimer Laser Ablated SrBi2Nb2O9 Thin Films. *Journal of Applied Physics*, **88**, 4294. https://doi.org/10.1063/1.1287782